ADVANCED OPTICAL MATERIALS
www.advopticalmat.de

Water-Induced and Wavelength-Dependent Light Absorption and Emission Dynamics in Triple-Cation Halide Perovskites

*John M. Howard, Kevin J. Palm, Qiong Wang, Erica Lee, Antonio Abate, Jeremy N. Munday, and Marina S. Leite**

Metal halide perovskites (MHP) can be made more stable through the addition of small amounts of cesium. Despite the improvement, these multication absorbers still display strong environmental sensitivity to any combination of factors, including water, oxygen, bias, temperature, and light. Here, the relationship is elucidated between light absorption, charge carrier radiative recombination, and relative humidity (rH) for the $Cs_{0.05}FA_{0.79}MA_{0.16}Pb(I_{0.83}Br_{0.17})_3$ composition, revealing partially reversible reductions in the extinction coefficient and fully reversible 25× enhancements in absolute light emission registered across the same humidity cycles up to 70% rH. With in situ excitation wavelength-dependent measurements, irreversible changes are identified in the perovskite after a single cycle of humidity-dependent photoluminescence (PL) performed with 450 nm excitation. The in situ measurement platform can be extended to test the effect of other stressors on thin films' optical behavior.

1. Introduction

Inthe last decade, metal halide perovskites (MHP) have emerged as the most promising class of optoelectronic materials, with broad applications in photovoltaics (PV) and light-emitting diodes (LED). Today, the limited long-term stability of MHP solar materials significantly limits commercial deployment.[1,2] Exposure to any combination of intrinsic (bias, temperature, and light) or extrinsic (water and oxygen) environmental stressors initiates changes in the fundamental optical and electronic properties,[3] typically followed by decreasing power conversion efficiency.[4] In perovskites, charge carrier recombination processes, and thus the photoluminescence (PL) signal, depend on composition, illumination conditions, and ambient environment,[5] with short durations oxygen and moderate humidity exposure increasing the overall quantum yield[6] and higher moisture concentrations leading to hydrated phases[7,8] and macroscopic degradation.[9] Accordingly, the use of in situ PL measurements to study the dynamics of charge carrier recombination is essential to develop a fundamental understanding of the photophysics governing the transient behavior presented by MHP devices.

Given that the economic prospects of MHP are contingent on long-term performance, optoelectronic stability has become one of the most prominent research foci within the perovskite scientific community.[10–12] Solving this problem requires physical insight into the degradation pathways[13–15] and the ability to mitigate material deterioration through compositional engineering.[16–19] Fundamental studies and fabrication refinements must occur in tandem and be systematically applied to hasten the search for stable perovskite films.[20–22] One of the larger victories produced by compositional engineering is the exploration of different cations at the A-site of the ABX_3 perovskite structure.[16,23–25] Chemical substitution of the A-site cation controls the structural

J. M. Howard, E. Lee
Department of Materials Science and Engineering
University of Maryland
College Park, MD 20742, USA

J. M. Howard, K. J. Palm, E. Lee
Institute for Research in Electronics and Applied Physics
University of Maryland
College Park, MD 20742, USA

K. J. Palm
Department of Physics
University of Maryland
College Park, MD 20742, USA

The ORCID identification number(s) for the author(s) of this article can be found under https://doi.org/10.1002/adom.202100710.

DOI: 10.1002/adom.202100710

Q. Wang, A. Abate
Helmholtz-Zentrum Berlin für Materialien und Energie
Kekuléstraße 5, 12489 Berlin, Germany

A. Abate
Department of Chemical, Materials and Production Engineering
University of Naples Federico II
Piazzale Tecchio 80, Fuorigrotta, Naples 80125, Italy

J. N. Munday
Department of Electrical and Computer Engineering
University of California
Davis, CA 95616, USA

M. S. Leite
Department of Materials Science and Engineering
University of California
Davis, CA 95616, USA
E-mail: mleite@ucdavis.edu

tolerance factor, providing a design guide for more robust MHP materials.[26] In particular, the use of three cations, formamidinium (FA), methylammonium (MA), and Cesium (Cs), has shown incredible benefit in promoting temperature stability up to 130 °C and lowering the *J–V* hysteresis, culminating in higher long-term performance devices.[4,16,27] Mixed-cation MHP materials have also enabled the fabrication of widely tunable (blue to near-infrafred) light-emitting diodes with increased EQE.[28,29] However, advancements in the community's understanding of the fundamental science surrounding the material stability have not kept pace with improved fabrication, highlighting a large opportunity for impactful research into the environmentally-driven optical and electrical dynamics in mixed-cation perovskites. Prior insight into the photophysics of FA-and MA-based perovskites[6,30–32] is not easily transferrable, requiring in situ measurements of these new compositions.[33]

Here, we resolve the time-dependent relationship between rH, light absorption, and radiative recombination in $Cs_{0.05}FA_{0.79}MA_{0.16}Pb(I_{0.83}Br_{0.17})_3$ (triple-cation perovskites, E_g = 1.58 eV) thin films. Our measurements of the absorption spectra over multiple moisture cycles from 2% up to ≈70% rH reveal a partially reversible reduction of the extinction coefficient that is most notable for wavelengths ≤500 nm. To unfold the light emission dynamics, we implement in situ environmental PL by subjecting the triple-cation perovskites to the same rH-cycles. With insight into both light absorption and emission, we establish that the 25-fold gain in PL with 532 nm excitation is independent of changes in light absorption. With excitation wavelength-dependent experiments, we reveal 450 and 500 nm to have a limited rise in PL yield due to light-activated near-surface decomposition. Subsequent rH-cycles with longer wavelengths fail to promote increased light emission beyond ≈2×. Our combined measurement-analysis framework establishes a standard approach to elucidate key structure-property relationships for metal halide perovskites that will aid the discovery of stable MHP compositions.

2. In situ Ellipsometry

The triple-cation perovskites investigated here are an ideal model system as this chemical composition delivers PV devices with high power conversion efficiency (>17%) with external quantum efficiency (EQE) >80% across the visible to near infrared spectrum. The champion solar cell presents minimal *J–V* hysteresis, as shown in **Figure 1**a. The perovskite layer is composed by compact grains ≈200 nm in diameter. The addition of Cs has been shown to yield a spatially uniform voltage response, despite the polycrystalline morphology.[33] Clearly, efforts to improve electrical performance have succeeded,[34] even at the nanoscale[33] as compared to prior devices.[35,36] Still, these triple-cation devices have not entirely eliminated the dynamic optical behavior observed in $MAPbI_3$ and $FAPbI_3$,[6,37] as we investigate with in situ humidity-dependent ellipsometry and PL measurements below. We choose to perform the in situ optical measurements on thin films (and not full devices) to elucidate the influence of incident photon energy on the moisture-induced response of the material, without any interface-convoluted effects. Yet, the films used in this analysis do produce state-of-the-art devices, as presented in Figure 1. Therefore, their optical response upon exposure to relative humidity (rH) is indeed a characteristic that will likely affect optoelectronic device performance.

To understand how water impacts the depth at which charge carriers are generated, we measure the absorption spectra over three sequential rH cycles from 0% to 75% in a nitrogen atmosphere, as shown in **Figure 2**. For this experiment we implement variable angle spectroscopic ellipsometry with in situ environmental control.[38] Here, the difference in polarization of light reflected off the sample surface is used to compute the refractive index (n) and extinction coefficient (k)—see Figures S1 and S2 in the Supporting Information. The latter is directly proportional to the absorption coefficient [$\alpha(\lambda) = 4\pi k/\lambda$]. Our ellipsometry measurements were performed in dynamic mode at three angles (55°, 70°, and 75°), with a spectrum acquired every ≈6 s (see Figure S3 (Supporting Information) for calibration data acquired from an Au thin film, used

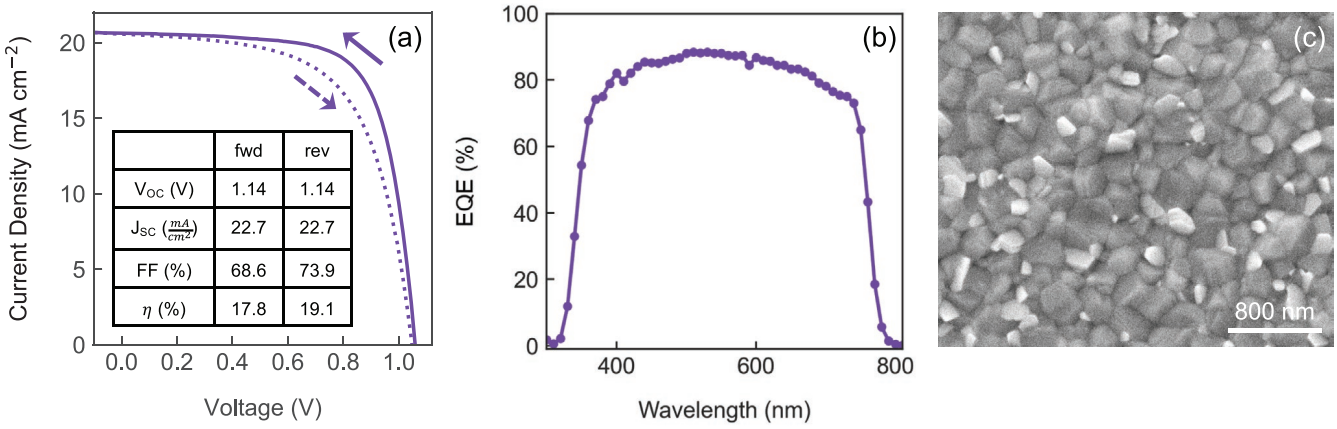

Figure 1. Photovoltaic performance of Cs-mixed perovskites. a) *J–V* characteristic of the best-performing triple-cation perovskite solar cell for reverse (dashed) and forward (solid) scan directions. Scan rate: 50 mV s^{-1}. b) External quantum efficiency (EQE) of the same device. Both *J–V* and EQE were acquired under AM1.5G illumination. c) Scanning electron micrograph (SEM) of the triple-cation perovskite grains.

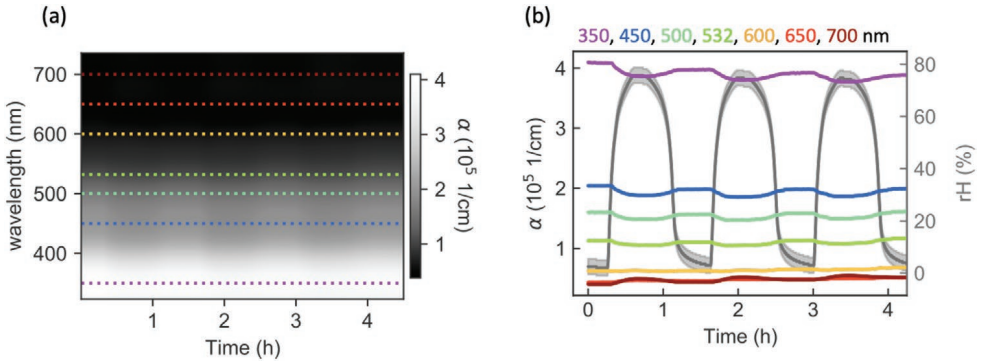

Figure 2. Humidity leads to partially reversible reduction in light absorption. a) 2D pseudocolor plot of the absorption coefficient (α) as a function of time over three humidity cycles. b) α for 350 nm (purple), 450 nm (blue), 500 nm (teal), 532 nm (green), 600 nm (orange), 650 nm (red), and 700 nm (burgundy) photons.

as a reference measurement). As shown in Figure 2a, humidity does not strongly impact the absorption spectrum, with only a faint indication of its rise and fall due to water vapor. Still, absorption is more greatly reduced for shorter wavelengths. To more closely examine the behavior, we selected representative wavelengths (350, 450, 500, 532, 600, and 700 nm) and tracked their evolution across the three cycles. Figure 2b displays the time-dependent. For shorter wavelengths (350–532 nm) a trend emerges, with α inversely correlated with the humidity level for rH >50%. Exposure to 70% rH (gray markers) drives the absorption slightly down to a local minimum before recovering almost fully just prior the start of the next humidity cycle. The oscillating behavior continues over subsequent rH cycles, accompanied by an overall decreasing trend in α as material degradation lessens the extent of recovery. Absorption at 600 nm and above is essentially unchanged throughout the course of the measurement with minor fluctuations that could be related to drift during the in situ ellipsometry measurements. The precise origin of the wavelength dependent behavior, i.e., α response as a function of wavelength, is not fully understood at this stage. Yet, our absorption measurements provide direct evidence that degradation in triple-cation perovskites is concentrated at the surface, given the more extensive reduction in the absorption coefficient at higher photon energies. Photolysis of residual PbI_2 (bandgap at ≈2.4 eV[39]) does not noticeably contribute to the diminishing absorption for higher humidity.[40] Instead, the adsorption of water decreases photon absorption at the sample surface region.

3. In situ Photoluminescence

We capture the influence of moisture on radiative recombination dynamics by submitting pristine triple-cation films to humidity-dependent PL experiments (**Figure 3**). Prior to all measurement, the samples were kept under a constant flow

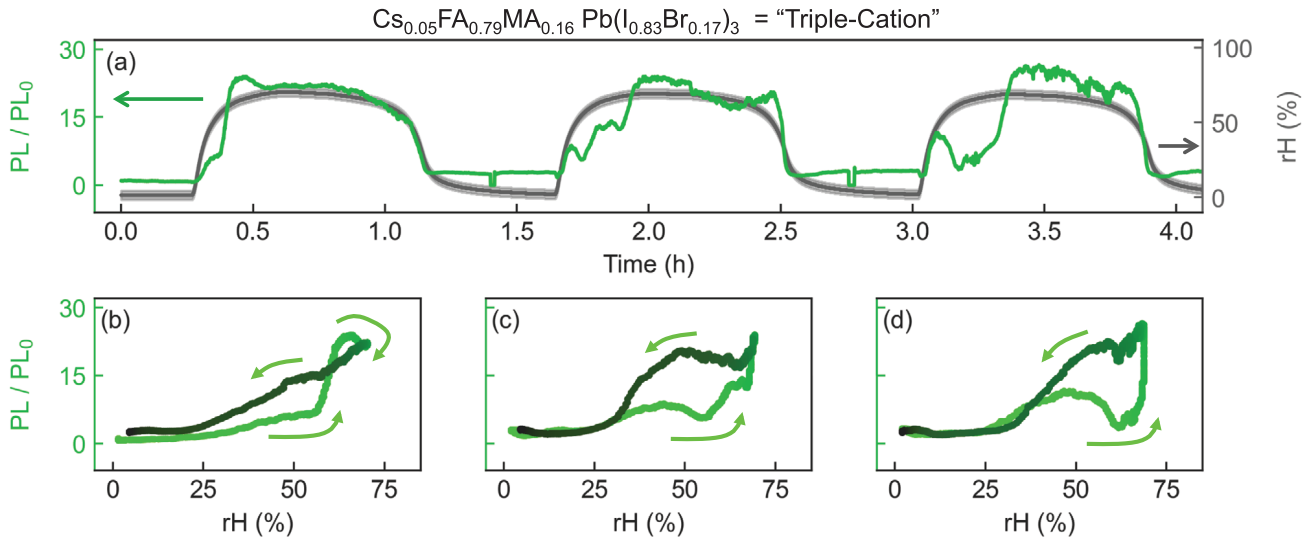

Figure 3. The presence of moisture greatly increases the photoluminescence (PL) intensity in triple-cation perovskites. a) rH (gray) and PL/PL_0 (green) as a function of time across three sequential and identical moisture cycles. b–d) PL/PL_0 rH-loops extracted from each of the three cycles capture the extent of hysteresis due to the influence of water on recombination. PL_0 is the initial value (PL ($t = 0$)). Excitation source: 532 nm at 3500 mW cm^{-2} (9.47×10^{22} photons s^{-1} m^{-2}).

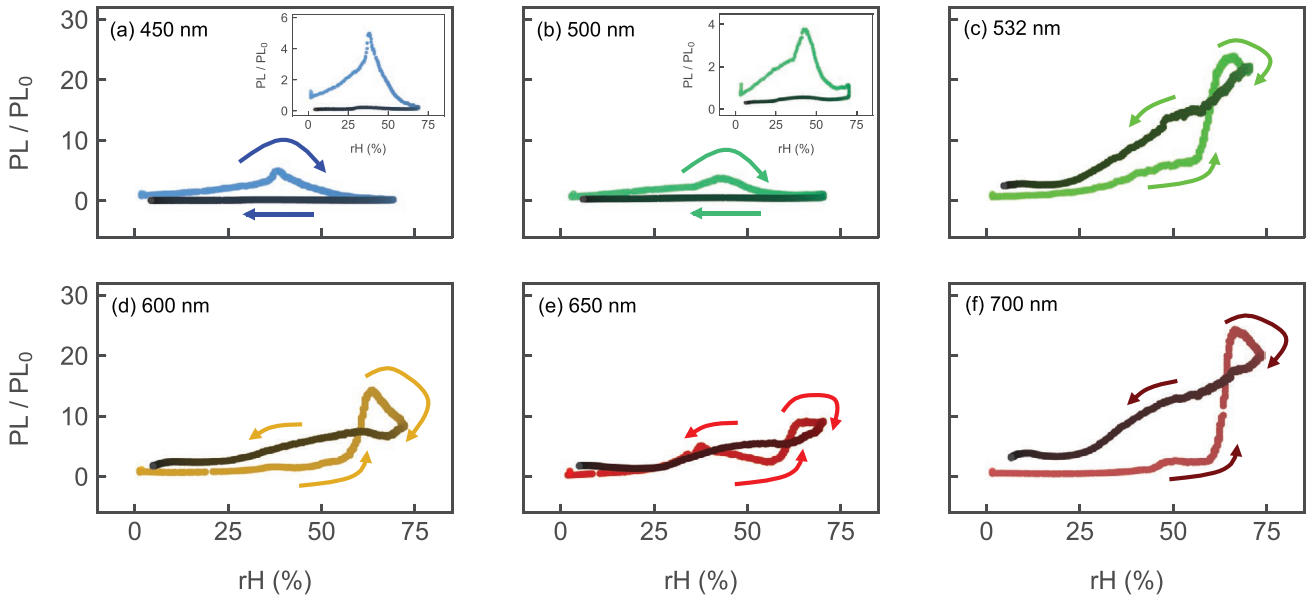

Figure 4. Humidity–photoluminescence hysteresis impacted by excitation photon energy. PL/PL_0 as a function of relative humidity (rH) for a) 450, b) 500, c) 532, d) 600, e) 650, and f) 700 nm excitation wavelengths. All measurements were performed with a uniform incident photon flux of 9.47×10^{22} photons s^{-1} m^{-2} and a fresh perovskite sample was measured for each wavelength.

of N_2 in the dark. As shown in Figure 3a, during the initial 0.25 h of the measurement, the perovskite films display an average ≈20% decrease in light emission below their initial values (see Figure S4b (Supporting Information) for the second dataset and Figure S5b (Supporting Information) for a zoomed view) despite the inert environment. Once moisture is introduced into the chamber, on average, the PL emission doubles in 18 min (28% rH) and eventually exhibits a ≈25× increase at >65% rH after 32 min (Figure 3a). The additional dataset for similar films presented in Figure S4 (Supporting Information) confirms the trend. Large rises in PL have been established in multiple compositions,[6,30] with prior measurements of $FAPbI_3$ films light emission escalating up to 140× in moist ambient air with UV excitation.[32] The upsurge in absolute PL yield may actually exceed 25×, given that any halide segregation leads to redshifting[41] and our detector's quantum efficiency drops in the near-infrared. For each subsequent cycle, the light emission takes longer to reach the maximum value, suggesting that moisture alters the chemistry of the film surface. To account for the large growth in PL emission, we suggest that water molecules passivate surface trap states and enable limited local halide segregation, promote highly efficient radiative recombination.[5,6] Interestingly, the rH-PL dynamics observed are completely reversible despite the repeated ≈25× enhancements. The inclusion of Cs has been shown to stabilize both films and full devices alike due to an increase in structural stability.[42] The large rise in radiative recombination may indicate that the addition of moisture to the precursor or during heat treatment may yield similar benefits to performance as realized in the $MAPbI_3$ and Cs-FA systems.[43] It is important to note that the measurements presented here significantly different than the ones previously reported for the Cs-FA family,[5] although they both present hysteresis. First, in the former the perovskites were aged in humidified nitrogen up to 70% rH while the in the latter we used humidified air up to 55% (containing oxygen). Second, the timing of the rH loops was also different. Here we employed continuous and symmetric humidity cycle with a 10 min hold at 70% rH; for our prior work each discrete humidity level was held for ≈50 min. Overall, regardless of the extent of the PL escalation, the full reversibility of the light emission dynamics further corroborates the claim that multiple A-site cations increases material stability.[16]

The relationship between rH and light emission is directly observed in Figure 3b–d, with the enclosed hysteresis loop revealing the influence of water adsorption for each cycle. For every rH-PL cycle, the color gradient indicates the order of the measurements in time, with earlier points taking a lighter green shade. For the first cycle, the interaction of water molecules with the perovskite lattice only becomes pronounced beyond 50% rH. The gradual rise in PL for rH <50% observed here may be attributable to physisorption that proceeds more slowly due to the presence of Cs. The first rH cycle is unique, given that the sample has not yet been subjected to any illumination or humidity. The initial exposure leads to a small secondary loop in the rH-PL characteristic that occurs due to the pristine film's heightened sensitivity to water vapor. All subsequent cycles (second and third in Figure 3c,d, respectively) require >50% rH to register the same ≈25× PL enhancement and do not display a secondary loop pattern. Our measurements have a sensitivity of ≈1% PL_0, indicating the significance of the observed difference between the initial and latter humidity cycles. Dehydration in the triple-cation film proceeds more slowly than hydration, as inferred by the more gradual declination in PL intensity and the resulting hysteresis loop. Critically, the magnitude of hysteresis measured upon completion of the cycle is minimal, indicating the full reversibility of the PL dynamics despite slower dehydration. While the presence of Cs reduces the lattice constant of the perovskite

structure, and thus ion migration and J–V hysteresis,[16,26,44] it also strengthens water adsorption and leads to a delayed decrease in absolute light emission.

We then assess the influence of rH for different charge carrier generation volumes, obtained by altering the excitation wavelength (450–700 nm) while maintaining a constant photon flux (**Figure 4**, raw time series in Figure S6 in the Supporting Information). A fresh, unexposed sample is used for each measurement. The higher energy photons have larger absorption coefficients, concentrating the generation of charge carriers in a smaller volume of the material, closer to the top surface. We choose to use a constant photon flux for each cycle to maintain approximately the same population of charge carriers across of all measurements. The absorption data acquired via ellipsometry indicates a 50% increase in generation rate for wavelengths ≤500 nm within the first 10 nm of the perovskite film. The impact of the higher charge carrier density is stark, with both 450 and 500 nm measurements showing minimal change in the PL signal, reaching only 5.0× and 3.8× their initial value, respectively. We hypothesize that the PL dynamics are reduced for shorter excitation wavelengths due to the PbI_2 segregated after fabrication (with E_g = 2.3–2.5 eV[39,45]). As previously shown for pure $MAPbI_3$, the photolysis reactions associated with PbI_2 provide two decomposition pathways: (i) the generation of Pb^0 and I_2 from PbI_2 photolysis and (ii) the formation of additional I_2 due to reactions between photogenerated holes with interstitial or film iodide.[40] The claim that photogenerated carriers from residual PbI_2 reduce PL dynamics is strongly supported by the large increase in PL at high rH values for excitation >520 nm (Figure 4c–f). All wavelengths beyond 520 nm exhibit PL enhancements at least double those observed for 450 and 500 nm. Additionally, a regime shift in the rH-PL behavior is observed around this characteristic wavelength. Combined exposure to humidity and 450 and 500 nm excitation leads to severe reductions in radiative recombination (90% and 70%, respectively) after just one cycle. In juxtaposition, all four other wavelengths display the characteristic pattern introduced in Figure 2 with an average 2.3× increase in PL at the end of the cycle. The light emission gradually grows with humidity up to 50% rH, after which the PL signal rises abruptly. Once the humidity stabilizes, the PL plateaus or slightly decreases. For a direct comparison of the initial emission rate of resulting from each excitation energy, we provide PL_0 for all wavelengths (in counts): 56.4 for 450 nm, 99.4 for 500 nm, 90.8 for 532 nm, 78.6 for 600 nm, 208.4 for 650 nm, and 152.5 for 700 nm. The PL enhancements revealed by our measurements for excitation wavelengths greater than 532 nm are due to reversible surface passivation and not because of halide segregation (minimal for the composition in question). The change in the surface layer only notably impacts the charge radiative recombination but not light absorption, as supported by the ellipsometry measurements. We note that the light conditions, in terms of overall intensity for the ellipsometry experiments, is not identical to the PL measurements performed in this work.

Given the negligible increase in radiative recombination when using 450 nm illumination, we perform the same series of measurements on a single film to evaluate the extent of permanent surface alteration. As shown in Figure S7a (Supporting Information), exposing the film to 450 nm excitation registers only a 5× growth in PL intensity and raises nonradiative recombination near the sample surface. Further, all subsequent measurements are constrained to gain ≤2×, even when measured with 700 nm. A second set of equivalent measurements (Figure S8, Supporting Information) reveals nearly identical behavior. By contrast, multiple rH-cycles with 532 nm illumination (Figure S4, Supporting Information) show PL enhancements of ≈25× for each cycle. Importantly, the data displayed in Figure 4a,e, Figures S4b, S7, and S8 (Supporting Information) were all collected from the same sample cleaved into multiple pieces inside a N_2 filled glovebox, indicating that the illumination condition, not sample-to-sample variation, dictates the qualitative trend observed in the rH-PL response. The combination of high humidity (≈70% rH) and excitation wavelength ≤500 nm generates a large population of permanent and localized surface defect states. For all measurements after 450 nm, the influence of moisture concentration, though negligible, is still observable. While the environment humidifies, a gradual rise in PL at ≈30% rH is observable, though the abrupt increase beyond 50% rH is absent. When the moisture is removed from the sample atmosphere, the PL sharply drops at ≈35% rH. The extent of the PL enhancement is correlated with excitation wavelength, suggesting that the new defects do not span the entire depth of the absorber. Optical micrographs acquired before and after each cycle (Figures S7g–m and S8g–m, Supporting Information) provide direct evidence of the perovskite surface modification at the location where the sample was illuminated (laser beam size was equal to ≈1 µm). Overall, moisture acts as an accelerant to the degradation of the perovskite surface. Our results are consistent with prior observations in Cs-FA perovskites.[4,5] Figure S7h in the Supporting Information reveals negligible alteration to the sample surface, suggesting that the new surface trap states that constrain light emission for 450 and 500 nm excitations were induced prior to the formation of the dark spot. Importantly, these dark spots do not form across the sample surface, but only where the laser is incident. A similar dark spot emerged (Figure S9, Supporting Information) for the triple rH-cycle measurements performed with 532 nm excitation (Figure 2), yet did not prevent the initial 25× increase in PL. Prior measurements of Cs-FA at twice the power density in oxygen further confirm that moisture acts to increase damage to the film.[5] The focused 450 nm laser illumination employed in Figures S7a and S8a (Supporting Information) has permanently altered the surface and potentially modified the crystal structure, as similar to previous reports for $MAPbI_3$.[46] Here, we propose that, unlike $MAPbI_3$, the presence of water is critical to drive the defect reactions responsible for the decline in PL.[17] We speculate that humidity >50% is sufficient to form a layer of water on the perovskite surface that acts as an *n*-type dopant, increasing the free electron density and weakening the Pb–I bonding.[47,48] The additional charge carriers provided by water adsorption accelerates the pace of the near-surface defect reactions that further limit PL. The length of the humidity cycle in our experiments acts to limit the extent to which water can deeply diffuse into the film, as supported by the similarity in PL hysteresis loops for wavelengths greater than 500 nm (Figures S7b–f and S8b–f, Supporting Information). Further measurements are required to fully understand the changes to the sample surface. For example, photoelectron

X-ray spectroscopy (XPS) of triple-cation thin films before and after soaking in high-humidity conditions (≥70% rH) under UV illumination could provide deeper insight into the chemical processes. To quantify the gradual changes to the film, we convert to its grayscale equivalent and present the histogram of the result. The transformation makes the broadening of the pixel values clear, with the rising left-hand side tail of the distribution corresponding to the growth of the black spot.

4. Conclusions

In summary, we temporally resolved the moisture-driven light absorption and emission dynamics in triple-cation halide perovskite films. Through dynamic in situ ellipsometry, we demonstrate partially reversible decreases to the absorption coefficient for wavelengths ≤600 nm, resulting from degradation of the near-surface region of the perovskite absorber. For the same humidity cycles, we established reversible and repeatable >25-fold increases in absolute PL intensity above 28% rH. The rH-PL hysteresis loops establish that >25-fold increase takes longer for each subsequent cycle, as the surface sensitivity of the thin film decreases due to localized decomposition. Through excitation wavelength-dependent PL measurements, we found 450 mn and 500 nm photons to only yield 5.0× and 3.8× gains in intensity, due to decomposition reactions driven by residual PbI_2. The rH-PL hysteresis loops for the wavelength-dependent series indicate that shorter wavelengths degrade the radiative recombination of the films. Our measurements establish the irreversible impact of short-wavelength excitation on the triple-cation films, with PL enhancement ≤2.1× after exposure to one cycle (≈1.35 h) of 450 nm. As an ensemble, our results reveal a delicate balance between moisture-based passivation treatments that improve radiative performance and the ability of water to degrade the film by creating new near-surface defects.

5. Experimental Section

Substrate Preparation: Both microscope slides and fluorine-doped tin oxide (FTO) substrates were cleaned prior to subsequent deposition steps. First, the substrates were sonicated in soap water (15 min), followed by a mixture of isopropanol (IPA) and acetone (15 min). Finally, a UV-ozone treatment was applied (15 min).

Electron Transport Layer Deposition: The compact TiO_2 layer was prepared with spray pyrolysis (450 °C) using a solution consisting of 0.72 mL titanium diisopropoxide bis(acetylacetonate) and 0.48 mL acetylacetone in 10.8 mL ethanol, sufficient for 24 substrates measuring 6.25 cm^2. The mesoporous TiO_2 was deposited with spin coating (4000 rpm for 10 s) from a dilute paste (125 g TiO_2 per L of ethanol), finished with a 30 min anneal at 450 °C.

CsFAMA Perovskite Thin Film Deposition: 1.5 M stock solution of PbI_2 and $PbBr_2$ was prepared in the mixture solvent of DMF and DMSO at the volume ratio of 4 to 1. 1.5 M stock solution of CsI was prepared in pure DMSO. Then, 0.05 g of MABr was dissolved in 347 µL $PbBr_2$ stock solution with the addition of 13 µL mixture solvent. 0.25 g of FAI was dissolved in 1169 µL PbI_2 stock solution with the addition of 3 µL mixture solvent. Then 1100 µL $FAPbI_3$ was mixed with 225.3 µL $MAPbBr_3$ and 69.8 µL CsI, which gives CsFAMA perovskite precursor solution of 1.24 M. Then 80 µL perovskite precursor was add to the substrate. The first spin-coating step raised the sample to 1000 rpm using an acceleration rate of 200 rpm per second and a dwell time of 5 s. The second spin-coating step increased the sample to 6000 rpm (acceleration: 3000 rpm s^{-1}) with a dwell time of 18 s. 100 µL chlorobenzene was added on top of the substrate 5 s before the end of the spin-coating program. The film was then finished on a hot plate at 100 °C for 60 min. All steps were completed within a nitrogen-filled glovebox.

Hole Transport Layer and Au Contact Deposition: First, 0.05 g of spiro-OMeTAD was added to 1383.1 µL of chlorobenzene. After, the following were added to the solution—20.19 µL of FK209 Co(III)TFSI (tris(2-(1*H*-pyrazol-1-yl)-4-tert-butylpyridine)cobalt(III) tri[bis(trifluoromethane)sulfonimide]) stock solution (300 mg mL^{-1} in acetonitrile), 19.92 µL of tBP (4-tert-Butypyridine), and 12.17 µL of LiTFSI (lithium bis(trifluoromethanesulfonyl)imide) stock solution (520mg mL^{-1} in acetonitrile). With spin coating (1800 rpm for 30 s, 200 rpm s^{-1} acceleration), the mixture was deposited on to the Cs, FA, MA perovskite. The samples were then kept in a dry air box overnight prior to adding the gold contacts. Then, 80 nm of gold was added via thermal evaporation (1×10^{-6} bar), yielding 0.144 cm^2 active area devices.

J–V Characterization: The *J–V* measurements were performed with a programmatically controlled sourcemeter, using a scan rate of 0.05 V s^{-1}. The 100 mW cm^{-2} light intensity was calibrated using a Silicon reference solar cell.

Humidity Control: Custom-built ellipsometry and microscopy chambers containing a capacitive humidity sensor was used to control the sample environment.[5,38] All samples were loaded into the enclosure while inside a glovebox. Once mounted on the microscope stage, dry N_2 was introduced into the chamber. The rH level was modulated by altering the flow rate of a separate N_2 line through a water bubbler using a mass flow controller (MFC) and measured via a sensor (±3% rH) embedded in the enclosure, as described in details in ref. [5]. All measurements were performed with the same setpoint ramp cycle applied by the MFC. During the entirety of our measurements the chamber temperature was constant (27.6 ± 0.2 °C), as displayed in Figure S10 in the Supporting Information. The chambers used for both in situ measurements have volume below 200 cc and the sensor is located within 1″ of the sample.

In Situ Variable Angle Spectroscopic Ellipsometry: Optical characterization of the samples was completed with spectroscopic ellipsometry (Woolam M-2000) in a custom built environmental chamber.[38] The perovskite samples were loaded into the environmental chamber inside an Ar glove box. The chamber was sealed before removal from the glove box to ensure the samples were never exposed to O_2 or any other contaminants. The chamber was then hooked up to the rH setup with dry N_2 flowing to the chamber. The initial optical properties under these conditions were measured. A dynamic ellipsometric measurement was then taken (six data points per minute) as the sample was exposed to the rH cycling described above. The dynamic measurement can only be recorded at one angle at a time, so these measurements were taken on three different samples from the same perovskite deposition, one sample for each of the three measurement angles (55°, 70°, 75°).

The ellipsometric data is fit using the Woollam CompleteEASE fitting software. The initial properties of the perovskite using all three-measurement angles are fit using a Kramers–Kronig consistent B-spline with 0.05 eV node spacing (Figure S1, Supporting Information). The thickness of the perovskite was found to be ≈520 nm with a roughness of ≈10 nm, which was in the range expected from the deposition parameters. In this fit, we must account for the change in the phase difference between TE and TM polarizations as light passes through the chamber windows (ellipsometric retardation effects). For each of the three measurement angles (55°, 70°, 75°), the retardation effects are fit as a free parameter using the following equation

$$\Delta(f) = f(C_1) \tag{1}$$

where Δ is the frequency-dependent retardation effects input to the model, f is the optical frequency of the spectroscopic beam, and C_1 is a fitting parameter. The origin of this retardation is the birefringence in the glass produced by anisotropic window stress when mounting the chamber lid. This retardation factor has been found to be constant

throughout the duration of an experiment. For the dynamic fitting, the thickness of the film was set to be constant and the B-spline parameters were allowed to refit for each time interval. The roughness was also allowed to refit in the range of 10–15 nm to account for slight expansion and roughening of the surface due to any H_2O being absorbed into the surface layer.[49] The initial conditions of each new B-spline fit were defined to be the fit from the previous time slice to ensure a smooth transition. Each individual dynamic angle was fit separately, using the same initial optical properties from the initial multi-angle fit. The dynamic optical properties calculated from each angle were then averaged to create the final reported values (Figure S2, Supporting Information).

In Situ Photoluminescence: A confocal microscope was used for all PL measurements. A super-continuum laser provided wavelength-dependent excitation; otherwise, a 532 nm power-tunable diode laser was used. For either laser source, the light was chopped at 150 Hz and cleaned with a 750 nm short-pass filter, before being coupled into an optical fiber with an adjustable parabolic mirror. The 532 nm diode laser spectrum was also cleaned with a 40 nm wide (FWHM) 550 nm center wavelength bandpass filter. The laser was focused by the microscope objective (100x, 0.75 N.A.) onto the sample mounted in a custom environmental enclosure. For measurements at all wavelengths, an incident photon flux of 9.47×10^{22} photons s^{-1} m^{-2} was used, implying a power density range of 2680–4170 mW cm^{-2} to account for the difference in the diffraction-limited spot size. The PL emission is collected by the same objective and detected by a photomultiplier tube (PMT) operated at 650 V. Any reflected laser light is blocked by a 750 nm long pass filter. The PMT output is read by a lock in amplifier. An optical micrograph was taken after each humidity cycle briefly blocking the PL signal.

Supporting Information

Supporting Information is available from the Wiley Online Library or from the author.

Acknowledgements

The authors thank N. Ballew and T. Weimar for their help in designing and machining the microscopy chamber, as well as Prof. Neves for fruitful discussions concerning the control of humidity. M.S.L. thanks the financial support from the National Science Foundation (ECCS awards #20-23974 and #16-10833). J.M.H. acknowledges the funding support from UMERC's 2018–2019 Harry K. Wells Graduate Fellowship, UMD's 2019 Graduate Summer Research Fellowship, and UMD's Fall 2019 Ann G. Wylie Dissertation Fellowship. K.J.P. is thankful for the support by a National Defense Science and Engineering Graduate Fellowship.

Conflict of Interest

The authors declare no conflict of interest.

Data Availability Statement

Research data are not shared.

Keywords

environmentally-dependent measurements, light absorption, metal halide perovskites, photoluminescence

Received: April 7, 2021
Revised: June 22, 2021
Published online:

[1] Z. Song, C. L. McElvany, A. B. Phillips, I. Celik, P. W. Krantz, S. C. Watthage, G. K. Liyanage, D. Apul, M. J. Heben, *Energy Environ. Sci.* **2017**, *10*, 1297.
[2] M. V. Khenkin, E. A. Katz, A. Abate, G. Bardizza, J. J. Berry, C. Brabec, F. Brunetti, V. Bulović, Q. Burlingame, A. Di Carlo, R. Cheacharoen, Y.-B. Cheng, A. Colsmann, S. Cros, K. Domanski, M. Dusza, C. J. Fell, S. R. Forrest, Y. Galagan, D. Di Girolamo, M. Grätzel, A. Hagfeldt, E. von Hauff, H. Hoppe, J. Kettle, H. Köbler, M. S. Leite, S. F. Liu, Y.-L. Loo, J. M. Luther, C.-Q. Ma, M. Madsen, M. Manceau, M. Matheron, M. McGehee, R. Meitzner, M. K. Nazeeruddin, A. F. Nogueira, Ç. Odabaşı, A. Osherov, N.-G. Park, M. O. Reese, F. De Rossi, M. Saliba, U. S. Schubert, H. J. Snaith, S. D. Stranks, W. Tress, P. A. Troshin, V. Turkovic, S. Veenstra, I. Visoly-Fisher, A. Walsh, T. Watson, H. Xie, R. Yıldırım, S. M. Zakeeruddin, K. Zhu, M. Lira-Cantu, *Nat. Energy* **2020**, *5*, 35.
[3] J. M. Howard, E. M. Tennyson, B. R. Neves, M. S. Leite, *Joule* **2019**, *3*, 325.
[4] K. Domanski, E. A. Alharbi, A. Hagfeldt, M. Grätzel, W. Tress, *Nat. Energy* **2018**, *3*, 61.
[5] J. M. Howard, E. M. Tennyson, S. Barik, R. Szostak, E. Waks, M. F. Toney, A. F. Nogueira, B. R. A. Neves, M. S. Leite, *J. Phys. Chem. Lett.* **2018**, *9*, 3463.
[6] R. Brenes, D. Guo, A. Osherov, N. K. Noel, C. Eames, E. M. Hutter, S. K. Pathak, F. Niroui, R. H. Friend, M. S. Islam, H. J. Snaith, V. Bulović, T. J. Savenije, S. D. Stranks, *Joule* **2017**, *1*, 155.
[7] A. M. A. Leguy, Y. Hu, M. Campoy-Quiles, M. I. Alonso, O. J. Weber, P. Azarhoosh, M. van Schilfgaarde, M. T. Weller, T. Bein, J. Nelson, P. Docampo, P. R. F. Barnes, *Chem. Mater.* **2015**, *27*, 3397.
[8] Z. Zhu, V. G. Hadjiev, Y. Rong, R. Guo, B. Cao, Z. Tang, F. Qin, Y. Li, Y. Wang, F. Hao, S. Venkatesan, W. Li, S. Baldelli, A. M. Guloy, H. Fang, Y. Hu, Y. Yao, Z. Wang, J. Bao, *Chem. Mater.* **2016**, *28*, 7385.
[9] J. A. Christians, P. A. Miranda Herrera, P. V. Kamat, *J. Am. Chem. Soc.* **2015**, *137*, 1530.
[10] T. A. Berhe, W.-N. Su, C.-H. Chen, C.-J. Pan, J.-H. Cheng, H.-M. Chen, M.-C. Tsai, L.-Y. Chen, A. A. Dubale, B.-J. Hwang, *Energy Environ. Sci.* **2016**, *9*, 323.
[11] T. Leijtens, K. Bush, R. Cheacharoen, R. Beal, A. Bowring, M. D. McGehee, *J. Mater. Chem. A* **2017**, *5*, 11483.
[12] L. Meng, J. You, Y. Yang, *Nat. Commun.* **2018**, *9*, 5265.
[13] Q. Wang, B. Chen, Y. Liu, Y. Deng, Y. Bai, Q. Dong, J. Huang, *Energy Environ. Sci.* **2017**, *10*, 516.
[14] G. Divitini, S. Cacovich, F. Matteocci, L. Cinà, A. Di Carlo, C. Ducati, *Nat. Energy* **2016**, *1*, 15012.
[15] M. Anaya, J. F. Galisteo-Lopez, M. E. Calvo, J. P. Espinos, H. Miguez, *J. Phys. Chem. Lett.* **2018**, *9*, 3891.
[16] M. Saliba, T. Matsui, J. Y. Seo, K. Domanski, J. P. Correa-Baena, M. K. Nazeeruddin, S. M. Zakeeruddin, W. Tress, A. Abate, A. Hagfeldt, M. Gratzel, *Energy Environ. Sci.* **2016**, *9*, 1989.
[17] S. G. Motti, D. Meggiolaro, A. J. Barker, E. Mosconi, C. A. R. Perini, J. M. Ball, M. Gandini, M. Kim, F. De Angelis, A. Petrozza, *Nat. Photonics* **2019**, *13*, 532.
[18] G. Grancini, C. Roldán-Carmona, I. Zimmermann, E. Mosconi, X. Lee, D. Martineau, S. Narbey, F. Oswald, F. De Angelis, M. Graetzel, M. K. Nazeeruddin, *Nat. Commun.* **2017**, *8*, 15684.
[19] S. Tan, I. Yavuz, N. De Marco, T. Huang, S.-J. Lee, C. S. Choi, M. Wang, S. Nuryyeva, R. Wang, Y. Zhao, H.-C. Wang, T.-H. Han,

B. Dunn, Y. Huang, J.-W. Lee, Y. Yang, *Adv. Mater.* **2020**, *32*, 1906995.
[20] J.-P. Correa-Baena, K. Hippalgaonkar, J. van Duren, S. Jaffer, V. R. Chandrasekhar, V. Stevanovic, C. Wadia, S. Guha, T. Buonassisi, *Joule* **2018**, *2*, 1410.
[21] S. Sun, N. T. P. Hartono, Z. D. Ren, F. Oviedo, A. M. Buscemi, M. Layurova, D. X. Chen, T. Ogunfunmi, J. Thapa, S. Ramasamy, C. Settens, B. L. DeCost, A. G. Kusne, Z. Liu, S. I. P. Tian, I. M. Peters, J.-P. Correa-Baena, T. Buonassisi, *Joule* **2019**, *3*, 1437.
[22] M. van Eerden, M. Jaysankar, A. Hadipour, T. Merckx, J. J. Schermer, T. Aernouts, J. Poortmans, U. W. Paetzold, *Adv. Opt. Mater.* **2017**, *5*, 1700151.
[23] G. E. Eperon, S. D. Stranks, C. Menelaou, M. B. Johnston, L. M. Herz, H. J. Snaith, *Energy Environ. Sci.* **2014**, *7*, 982.
[24] D. P. McMeekin, G. Sadoughi, W. Rehman, G. E. Eperon, M. Saliba, M. T. Horantner, A. Haghighirad, N. Sakai, L. Korte, B. Rech, M. B. Johnston, L. M. Herz, H. J. Snaith, *Science* **2016**, *351*, 151.
[25] Y. Wu, D. Yan, J. Peng, T. Duong, Y. Wan, S. P. Phang, H. Shen, N. Wu, C. Barugkin, X. Fu, S. Surve, D. Grant, D. Walter, T. P. White, K. R. Catchpole, K. J. Weber, *Energy Environ. Sci.* **2017**, *10*, 2472.
[26] Z. Li, M. Yang, J.-S. Park, S.-H. Wei, J. J. Berry, K. Zhu, *Chem. Mater.* **2015**, *28*, 284.
[27] J. A. Christians, P. Schulz, J. S. Tinkham, T. H. Schloemer, S. P. Harvey, B. J. Tremolet de Villers, A. Sellinger, J. J. Berry, J. M. Luther, *Nat. Energy* **2018**, *3*, 68.
[28] H. P. Kim, J. Kim, B. S. Kim, H.-M. Kim, J. Kim, A. R. b. M. Yusoff, J. Jang, M. K. Nazeeruddin, *Adv. Opt. Mater.* **2017**, *5*, 1600920.
[29] P. Vashishtha, S. A. Veldhuis, S. S. H. Dintakurti, N. L. Kelly, B. E. Griffith, A. A. M. Brown, M. S. Ansari, A. Bruno, N. Mathews, Y. Fang, T. White, S. G. Mhaisalkar, J. V. Hanna, *J. Mater. Chem. C* **2020**, *8*, 11805.
[30] Y. Tian, M. Peter, E. Unger, M. Abdellah, K. Zheng, T. Pullerits, A. Yartsev, V. Sundstrom, I. G. Scheblykin, *Phys. Chem. Chem. Phys.* **2015**, *17*, 24978.
[31] E. T. Hoke, D. J. Slotcavage, E. R. Dohner, A. R. Bowring, H. I. Karunadasa, M. D. McGehee, *Chem. Sci.* **2015**, *6*, 613.
[32] H.-H. Fang, F. Wang, S. Adjokatse, N. Zhao, M. A. Loi, *Adv. Funct. Mater.* **2016**, *26*, 4653.
[33] E. M. Tennyson, B. Roose, J. L. Garrett, C. Gong, J. N. Munday, A. Abate, M. S. Leite, *ACS Nano* **2018**, *13*, 1538.
[34] National Renewable Energy Lab, *Best Research-Cell Efficiency Chart NREL*, Washington, DC **2020**.
[35] J. L. Garrett, E. M. Tennyson, M. Hu, J. Huang, J. N. Munday, M. S. Leite, *Nano Lett.* **2017**, *17*, 2554.
[36] Y. Kutes, Y. Zhou, J. L. Bosse, J. Steffes, N. P. Padture, B. D. Huey, *Nano Lett.* **2016**, *16*, 3434.
[37] H. H. Fang, S. Adjokatse, H. T. Wei, J. Yang, G. R. Blake, J. S. Huang, J. Even, M. A. Loi, *Sci. Adv.* **2016**, *2*, e1600534.
[38] K. J. Palm, J. B. Murray, T. C. Narayan, J. N. Munday, *ACS Photonics* **2018**, *5*, 4677.
[39] R. Ahuja, H. Arwin, A. Ferreira da Silva, C. Persson, J. M. Osorio-Guillén, J. Souza de Almeida, C. Moyses Araujo, E. Veje, N. Veissid, C. An, *J. Appl. Phys.* **2002**, *92*, 7219.
[40] W.-A. Quitsch, D. W. deQuilettes, O. Pfingsten, A. Schmitz, S. Ognjanovic, S. Jariwala, S. Koch, M. Winterer, D. S. Ginger, G. Bacher, *J. Phys. Chem. Lett.* **2018**, *9*, 2062.
[41] S. Cacovich, D. Messou, A. Bercegol, S. Bechu, A. Yaiche, H. Shafique, J. Rousset, P. Schulz, M. Bouttemy, L. Lombez, *ACS Appl. Mater. Interfaces* **2020**, *12*, 34784.
[42] J.-W. Lee, D.-H. Kim, H.-S. Kim, S.-W. Seo, S. M. Cho, N.-G. Park, *Adv. Energy Mater.* **2015**, *5*, 1501310.
[43] G. E. Eperon, S. N. Habisreutinger, T. Leijtens, B. J. Bruijnaers, J. J. van Franeker, D. W. deQuilettes, S. Pathak, R. J. Sutton, G. Grancini, D. S. Ginger, R. A. Janssen, A. Petrozza, H. J. Snaith, *ACS Nano* **2015**, *9*, 9380.
[44] T. Matsui, J. Y. Seo, M. Saliba, S. M. Zakeeruddin, M. Grätzel, *Adv. Mater.* **2017**, *29*, 1606258.
[45] Y. Wang, Y.-Y. Sun, S. Zhang, T.-M. Lu, J. Shi, *Appl. Phys. Lett.* **2016**, *108*, 013105.
[46] N. Phung, A. Al-Ashouri, S. Meloni, A. Mattoni, S. Albrecht, E. L. Unger, A. Merdasa, A. Abate, *Adv. Energy Mater.* **2020**, *10*, 1903735.
[47] Y. Li, X. Xu, C. Wang, C. Wang, F. Xie, J. Yang, Y. Gao, *J. Phys. Chem. C* **2015**, *119*, 23996.
[48] Z. Song, N. Shrestha, S. C. Watthage, G. K. Liyanage, Z. S. Almutawah, R. H. Ahangharnejhad, A. B. Phillips, R. J. Ellingson, M. J. Heben, *J. Phys. Chem. Lett.* **2018**, *9*, 6312.
[49] Z. Zhu, V. G. Hadjiev, Y. Rong, R. Guo, B. Cao, Z. Tang, F. Qin, Y. Li, Y. Wang, F. Hao, S. Venkatesan, W. Li, S. Baldelli, A. M. Guloy, H. Fang, Y. Hu, Y. Yao, Z. Wang, J. Bao, *Chem. Mater.* **2016**, *20*, 7385.